

# Field-enhanced diamagnetism in intense magnetic field in the pseudogap state of the cuprate $\text{Bi}_2\text{Sr}_2\text{CaCu}_2\text{O}_{8+\delta}$

Yayu Wang<sup>1</sup>, Lu Li<sup>1</sup>, M. J. Naughton<sup>2</sup>, G. D. Gu<sup>3</sup>, S. Uchida<sup>4</sup>, N. P. Ong<sup>1</sup>

<sup>1</sup>*Department of Physics, Princeton University, New Jersey 08544, U.S.A.*

<sup>2</sup>*Department of Physics, Boston College, Chestnut Hill, Massachusetts 02467, U.S.A.*

<sup>3</sup>*Department of Physics, Brookhaven National Laboratory, Upton, N.Y. 11973.*

<sup>4</sup>*School of Frontier Science, University of Tokyo, Tokyo 113-8656, Japan.*

(Dated: June 24, 2018)

In hole-doped cuprates, Nernst experiments imply that the superconducting state is destroyed by spontaneous creation of vortices which destroy phase coherence. Using torque magnetometry on  $\text{Bi}_2\text{Sr}_2\text{CaCu}_2\text{O}_{8+\delta}$ , we uncover a field-enhanced diamagnetic signal  $M$  above the transition temperature  $T_c$  that increases with applied field to 32 Tesla and scales just like the Nernst signal. The magnetization results above  $T_c$  distinguish  $M$  from conventional amplitude fluctuations, and strongly support the vortex scenario for the loss of phase coherence at  $T_c$ .

PACS numbers: 74.25.Dw, 74.72.Hs, 74.25.Ha

In conventional superconductors, the superconducting transition involves vanishing of the macroscopic wave function  $\hat{\Psi}$ , but in hole-doped cuprates there is growing evidence that the transition is caused by the proliferation of vortices which destroy long-range phase coherence. The detection of a large Nernst signal  $e_N$  and kinetic inductance above the critical transition temperature  $T_c$  has provided evidence for the vortex scenario [1, 2, 3, 4, 5, 6], but there should exist a magnetic signature. Despite the loss of phase coherence above  $T_c$ , one should observe a weak magnetization  $M$  that differs qualitatively from ‘fluctuation diamagnetism’ observed in low- $T_c$  superconductors. However, the magnetization evidence to date is ambiguous. Using high-field, high-resolution torque magnetometry on  $\text{Bi}_2\text{Sr}_2\text{CaCu}_2\text{O}_{8+\delta}$  (Bi 2212), we show the existence of a field-enhanced diamagnetism above  $T_c$  that closely matches the Nernst signal as a function of both field  $H$  and temperature  $T$ . In addition to establishing the unusual nature of the transition and its diamagnetic state above  $T_c$ , we show that the upper critical field  $H_{c2}(T)$  remains very large at  $T_c$ , a behavior similar to that predicted for the Kosterlitz-Thouless (KT) transition [7].

Torque magnetometry measurements were performed on an underdoped (UD), an optimally-doped (OP) and an overdoped (OD) crystal of Bi 2212. Each crystal was glued to the tip of a Si cantilever with its  $c$ -axis at an angle  $\varphi_0 \sim 15^\circ$  to  $\mathbf{H}$  (Fig. 1a, inset). The torque  $\boldsymbol{\tau} = \mathbf{m} \times \mathbf{B}$  leads to a flexing of the cantilever which is detected capacitively, where  $\mathbf{m}$  is the sample’s magnetic moment and  $\mathbf{B} = \mu_0(\mathbf{H} + \mathbf{M})$  with  $\mu_0$  the vacuum permeability. We resolve  $m \sim 5 \times 10^{-9}$  emu at 10 T. Measurements were also performed in a SQUID magnetometer (with resolution  $\sim 10^{-6}$  emu). All curves of  $M$  reported here are *fully reversible* in  $H$  and  $T$ . Our high-field results, in combination with the Nernst effect, point to conclusions very different from those inferred from earlier torque experiments [8, 9, 10].

The torque curves measured in an underdoped (UD) Bi 2212 crystal, with  $T_c = 50$  K, are shown in Fig. 1a.

Above 120 K,  $\tau$  is dominated by a paramagnetic term that changes little from 200 to 120 K. Below 120 K, however, a diamagnetic term appears, and grows rapidly to pull the torque to large negative values.

We express the torque as an effective magnetization [8]  $M_{eff} \equiv \tau/B_x V$ , with  $V$  the sample volume and  $B_x = B \sin \varphi_0$  (we take  $\hat{\mathbf{z}} \parallel \hat{\mathbf{c}}$ ). For  $\varphi_0 \ll 1$ , we have  $M_{eff} = \Delta\chi H_z + M(T, H_z)$ , where  $M(T, H_z)$  is the magnetization of interest here. The paramagnetic background reflects the susceptibility anisotropy  $\Delta\chi = \chi_c - \chi_{ab}$ , which is the difference between the uniform susceptibilities  $\chi_c$  ( $\mathbf{H} \parallel \hat{\mathbf{c}}$ ) and  $\chi_{ab}$  ( $\mathbf{H} \perp \hat{\mathbf{c}}$ ). For either axis  $i$  ( $c$  or  $ab$ ),  $\chi_i$  is comprised of 3 terms, viz.  $\chi_i(T) = \chi_i^{core} + \chi_i^{orb} + \chi_i^s(T)$  [11, 12, 13]. The strongly anisotropic orbital (van Vleck) term  $\chi_i^{orb}$  gives the largest contribution to  $\Delta\chi$ , while the isotropic core term  $\chi_i^{core}$  gives zero. These 2 terms are  $T$  independent, but the spin susceptibility  $\chi_i^s(T)$  is  $T$  dependent. NMR (nuclear magnetic resonance) Knight-shift experiments [12, 13] reveal that, in UD cuprates,  $\chi_i^s(T)$  decreases below  $T^*$ , reflecting the growth of the spin gap. However, because the  $g$ -factor anisotropy is weak ( $g_c/g_{ab} \sim 1.14$ ), this translates to only a small,  $T$ -dependent correction to the large, constant van Vleck contribution in  $\Delta\chi$  (see analysis in Ref. [11]).

Consistent with this, our torque results reveal that the paramagnetic term  $\Delta\chi H_z$  is weakly  $T$  dependent in all samples tested. In  $\text{La}_{2-x}\text{Sr}_x\text{CuO}_4$  (LSCO) with  $x = 0.050$ , in which  $T_c < 2$  K and  $M(T)$  is not resolved above 25 K,  $M_{eff}(T) = \Delta\chi H_z$  changes by only  $\sim 6\%$  between 200 and 25 K (open circles in Fig. 1b). Likewise, in both Bi 2212 samples (solid symbols),  $M_{eff}(T) = \Delta\chi H_z$  shows a weak  $T$ -dependence from 200 K to 120 K which we fit to a straight line (dotted lines in Fig. 1b). We assume that  $\Delta\chi$  continues this linear behavior below  $T_{onset} \sim 120$  K where  $M(T, H_z)$  is first resolved, and measure  $M(T, H_z)$  relative to the dotted lines (shaded areas) [14]. Hereafter, we write  $H_z$  as  $H$ .

Figure 2 compares the curves of  $M(T, H)$  vs.  $H$  measured at fixed  $T$  in the UD and OP samples (Panels a and b, respectively). As  $T \rightarrow T_c$  (50 and 87.5 K, respec-

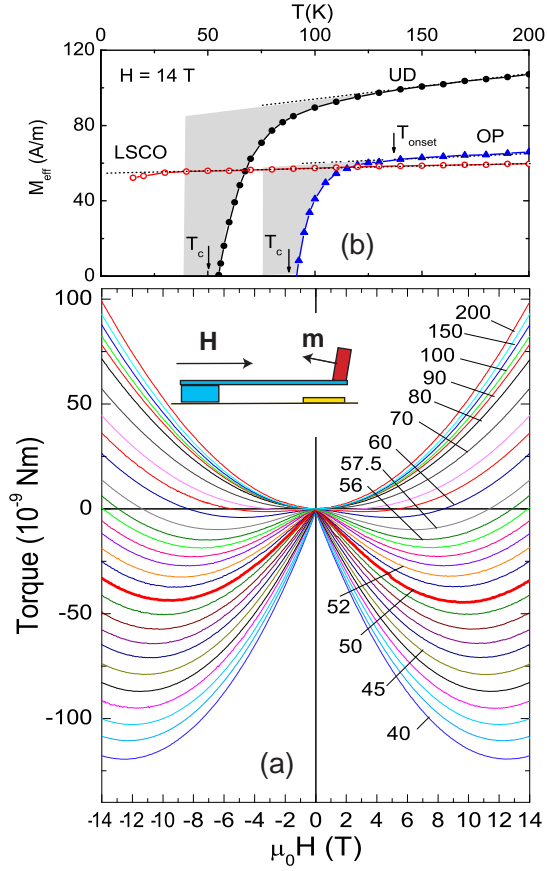


FIG. 1: (a) The measured torque  $\tau$  vs.  $H$  at selected  $T$  in UD Bi 2212 with  $T_c = 50$  K (crystal size  $\sim 0.2 \times 1 \times 1$  mm<sup>3</sup>). The parabolic behavior above 120 K arises from  $\Delta\chi H_z$ . Below 120 K, a diamagnetic contribution  $M$  grows rapidly. Measurements were extended to 32 T at selected  $T$ . The inset shows the cantilever. The maximum beam deflection is  $0.15^\circ$ . (b) The  $T$  dependence of  $M_{eff}$  in single-crystal UD and OP Bi 2212 (solid symbols) and in LSCO ( $x = 0.050$ , open circles) at  $B = 14$  T. The LSCO data show that  $\Delta\chi$  is only weakly  $T$ -dependent down to  $\sim 25$  K. In Bi 2212, the diamagnetic signal  $M(H_z)$  is shown shaded.

tively),  $M(T, H)$  grows over a broad interval (of width 70 K and 30 K, respectively). A feature of  $M$ , distinguishing it from the paramagnetic signal, is its pervasive nonlinearity versus  $H$  (analyzed in Ref. [15]). A second striking feature is that the curves 5–10 K above  $T_c$  are similar in form to that measured either at  $T_c$  (shown as bold curves) or a few K below. To show this more clearly, we plot in Figs. 2c and 2d  $M$  versus  $T$  with  $H$  fixed at values up to 32 T. Whereas the Meissner transition is quite sharp (curve at 10 Oe), the high-field curves vary smoothly across  $T_c$ .

Previously, measurements of  $M$  above  $T_c$  were largely identified [11, 16] with amplitude fluctuations  $\delta|\Psi|$ , in analogy with “fluctuation diamagnetism”  $M'$  in low- $T_c$  superconductors [17]. However, difficulties with this interpretation have been noted also [8, 9, 18, 19, 20].

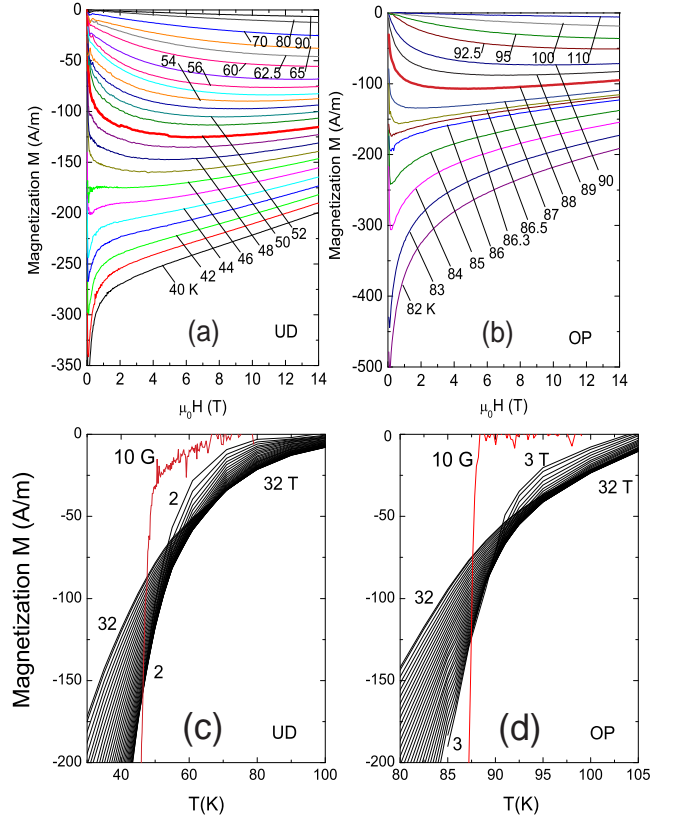


FIG. 2: Curves of magnetization  $M(T, H)$  plotted vs.  $H$  at selected  $T$  in the (Panels a and b), and plotted vs.  $T$  in (c and d) for the UD ( $T_c = 50$  K) and OP ( $T_c = 87.5$  K) samples. In (a) and (b), the bold curve is taken at  $T_c$ . In Panels (c) and (d), the  $T$  dependence of  $M$  is plotted at fixed  $H$  in the UD and OP sample, respectively [ $H$  decreases, in steps of 1 Tesla, from 32 T to 2 T in (a) and 3 T in (b)]. Curves labelled 10 G show the Meissner transition at  $T_c$  measured at  $H = 10$  Oe. In the UD sample, the foot above 50 K is a minority phase 2.5% in volume (see text). Increasing  $H$  to values 3–32 T greatly amplifies the diamagnetic signal in a broad interval above  $T_c$ .

We show next that the diamagnetism in Bi 2212 is actually qualitatively distinct from amplitude fluctuations. The evidence are of 3 types. First, we focus on  $T > T_c$ . As seen in Fig. 2, in a field of 32 T,  $M$  survives as a long tail over a 70-K interval (30-K interval) above  $T_c$  in the UD (OP) sample. This robustness in intense fields sharply distinguishes the cuprate signal from that in low- $T_c$  superconductors. To emphasize this important difference, we focus on the OP sample (Fig. 2d). With  $H = 10$  Oe,  $M$  displays a sharp Meissner transition at  $T_c = 87.5$  K. However, a field of 3 T “amplifies” the diamagnetic signal by  $\sim 3$  orders of magnitude rendering  $M$  observable to  $\sim 104$  K. Further increase of  $H$  to 32 T makes the signal visible to 120 K. The monotonic increase of  $M$  with  $H$  implies that the condensate is not destroyed in a 32-Tesla field, i.e. the depairing field  $H_{c2}$  lies significantly higher at these  $T$ . In the UD sample (Fig. 2c),

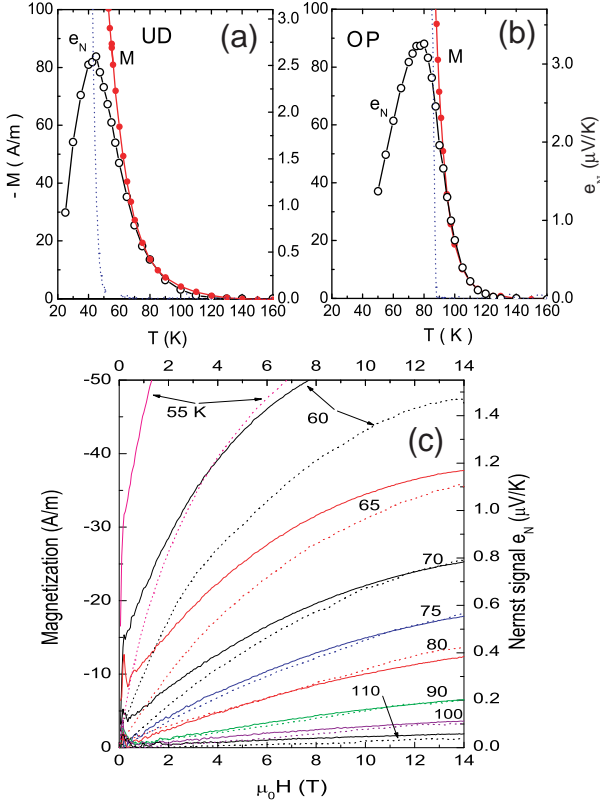


FIG. 3: Comparison of  $M$  and the vortex-Nernst signal  $e_N$  measured at 14 T in the UD (Panel a) and OP (b) Bi 2212, and comparison of their field profiles in UD Bi 2212 (Panel c). In Panels (a) and (b),  $M$  and  $e_N$  track each other at high  $T$ . Below  $T_c$ ,  $M$  increases rapidly while  $e_N$  attains a peak before falling towards zero in the vortex-solid phase. The dashed curves show  $M$  measured in  $H = 10$  Oe. Panel (c) shows that curves of  $M$  vs.  $H$  (solid curves) match those of  $e_N$  vs.  $H$  (dashed curves) in the UD sample above  $T_c$  (the scale factor between  $M$  and  $e_N$  is the same as in Panel a). The observed Nernst signal is the sum of the vortex contribution and a negative, quasiparticle (qp) term  $e_N^{obs} = e_N + e_N^{qp}$ . The curves show  $e_N$  after the small qp term is subtracted ( $|e_N^{qp}| < 0.04 \mu\text{V/K}$ ).

a phase of volume 2.5% (estimated from  $\chi$ ) with higher  $T_c \sim 70$  K is apparent as a “foot” extending from 50 to 70 K. As discussed below, this small phase does not affect our conclusions.

By contrast, in low- $T_c$  superconductors, the fluctuation signal  $M'$  from amplitude fluctuations is suppressed in weak  $H$ . In Nb,  $M'$  becomes unresolved above 1000 Oe (Fig. 13 of Ref. [17] for Nb, In and Pb and alloys). There the field sensitivity reflects the approach  $H_{c2}(T) \rightarrow 0$  at  $T_c$ , and the role of nonlocal electrodynamics in suppressing short-wavelength fluctuations.

Secondly, we show that the diamagnetic signal above  $T_c$  is closely related to the Nernst signal (measured in the same crystals). In Figs. 3a and 3b, we plot the  $T$  dependence of  $e_N$  and  $M$  (both at 14 T) in the UD and OP samples, respectively (the 10-Oe curves are shown

as dashed curves). Remarkably,  $M$  (solid circles) tracks  $e_N$  (open) over a broad interval of temperature before diverging near  $T_c$ . Below  $T_c$ ,  $M$  rises steeply whereas  $e_N$  attains a broad peak before decreasing towards zero (its value in the vortex solid phase). The 2 signals  $M$  and  $e_N$  share the same onset temperature  $T_{onset}$ .

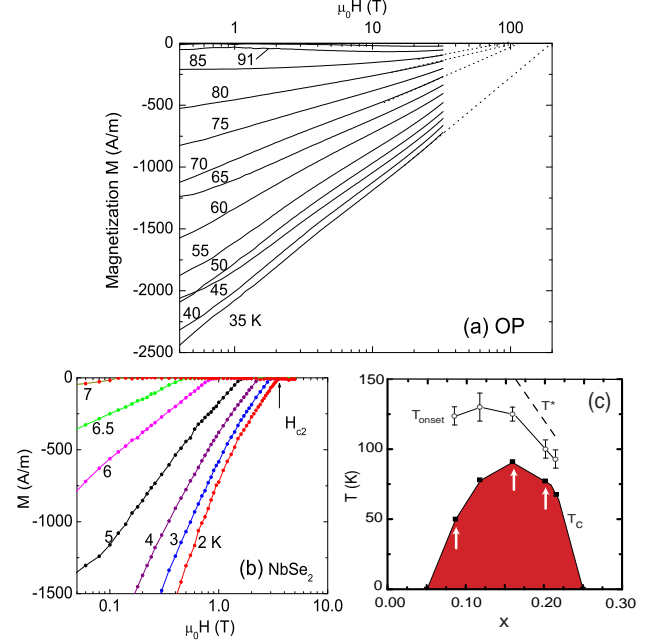


FIG. 4: Plot of the field dependence of  $M$  in OP Bi 2212 (Panel a) and in NbSe<sub>2</sub> (b) and the phase diagram of Bi 2212 (Panel c). In Panel a,  $|M|$  falls roughly linearly in  $\log H$  from 0.2 T to 32 T. The inferred  $H_{c2}(T)$  values stay above 90 T as  $T \rightarrow T_c$  ( $= 86$  K). In Panel b, the measured  $M$  also shows a nominally linear dependence on  $\log H$ . However, in contrast with (a),  $H_{c2}(T)$  decreases from 3.6 T to 0.12 T as  $T$  rises from 2 to 7 K. In Panel c,  $T_{onset}$  of both  $M$  and  $e_N$  is plotted vs.  $x$  (hole content) together with  $T_c$  and  $T^*$ . Arrows indicate the 3 samples studied by torque magnetometry.

In both samples, the direct proportionality between  $M$  and  $e_N$  above  $T_c$  also holds as  $H$  is varied. We compare their respective field profiles in the UD sample in Fig. 3c. Over the interval 70-120 K, we find that the  $M$  vs.  $H$  curves (solid) can be overlaid on the  $e_N$  vs.  $H$  curves (dashed) with the same scaling factor as in Fig. 3a. (Figure 3c also clarifies the contribution of the minority phase in the UD sample. At 60 and 65 K, the 2.5% phase adds a small term to  $M$  that is nearly constant in  $H$ . However, it does not contribute to  $e_N$  because it does not extend over the sample, so the curves of  $M$  lie slightly above  $e_N$  below 70 K. Above 70 K, this difference is unobservable. The 2.5% phase cannot account for the large diamagnetic signal extending to 120 K.) In terms of the resistivity  $\rho$  and  $\alpha_{yx} = J_y/|\nabla T|$ , we have  $e_N = \rho \alpha_{xy}$ , with  $J_y$  the transverse charge current. The scaling relationship [21] is then  $\alpha_{xy} = -\beta M$  for  $T > T_c$ . Figure 3 directly con-

firms that, above  $T_c$ , the growth of  $e_N$  is accompanied by an increase of the diamagnetic signal, as required by the vortex scenario.

Lastly, we describe the behavior of  $H_{c2}(T)$  inferred from the curves at  $T < T_c$  (Fig. 4a). In the extreme type II case, the high-field behavior  $M \sim -[H_{c2}(T) - H]$ , provides a reliable way to find  $H_{c2}(T)$ . In Fig. 4b we plot  $M$  in NbSe<sub>2</sub> (measured by SQUID) against  $\log H$ . As  $T \rightarrow T_c^-$ , the inferred values approach zero as  $H_{c2}(T) \sim (T_c - T)$ . The vanishing of  $H_{c2}(T)$  causes the amplitude fluctuations to be sensitive to field.

The curves of  $H_{c2}(T)$  in Bi 2212 behave in a qualitatively different way. Figure 4a plots the curves of  $M$  vs.  $\log H$  in the OP sample from 0.4 T to 32 T at temperatures 35 to 91 K. At each  $T$ , the decrease in  $M$  is nominally linear in  $\log H$ , but  $M$  clearly retains significant strength at 32 T. Assuming this linear dependence holds above 32 T (as the curves for NbSe<sub>2</sub> suggest), we may estimate  $H_{c2}$  using the dashed lines in Fig. 4a. The inferred values of  $H_{c2}$  decrease from 200 T at 35 K to the large value 90 T at  $T_c = 86$  K, instead of going to zero (in agreement with  $H_{c2}$  derived from  $e_N$  [4]). This unusual behavior of  $H_{c2}(T)$  – so strikingly different from the BCS scenario – is similar to that predicted for the KT transition [7, 22]. It seems to be a defining signature of the phase-disordering scenario.

The existence of a large  $e_N$  and  $M$  in an extended (“Nernst”) region above the  $T_c$  dome has important implications for the phase diagram and the pseudogap state [23]. First, the results support the proposal [24] that the curve of  $T_c$  vs.  $x$  reflects strong phase disordering, rather than the vanishing of  $\hat{\Psi}$ . Secondly, we

note that the curve of  $T_{onset}$  lies significantly lower than  $T^*$  (Fig. 4c), and has a different  $x$  dependence. The Nernst region  $T_c < T < T_{onset}$  is characterized by the existence of vorticity and weak diamagnetic currents. Above  $T_{onset}$ , however, these signatures vanish. Hence the high- $T$  region  $T_{onset} < T < T^*$  must harbor a type of broken-symmetry state in which only the spin degrees see a “spin-gap”, but supercurrents are absent. There are 2 distinct crossover temperatures: The local correlation that appears at  $T^*$  affects mostly the spin degrees, whereas vorticity and supercurrents appear at the lower  $T_{onset}$ .

Finally, the  $T_c$  curve is nested within the  $T_{onset}$  curve, which is nested, in turn, within the pseudogap region below  $T^*$ . This sequential nesting suggests that, despite the absence of supercurrents, the high-temperature pseudogap state is closely related to  $d$ -wave superconductivity. As  $T$  decreases from 300 K, the system gradually evolves from one to the other across the Nernst region. Recent interesting proposals describe this evolution as either spin-charge locking [25], fluctuations of the quantization axis  $\hat{I}$  in SU(2) theory [23, 26], or fluctuations of the “electron nematic” phase in the striped model [27].

The high-field measurements were performed at the National High Magnetic Field Laboratory, Tallahassee, which is supported by the U.S. National Science Foundation (NSF) and the State of Florida. This research is supported by NSF Grant DMR 0213706. GDG was supported by the DOE under contract No. DE-AC02-98CH10886.

- 
- [1] Z. A. Xu, N. P. Ong, Y. Wang, T. Kakeshita, S. Uchida, *Nature* **406**, 486 (2000).
  - [2] Yayu Wang *et al.*, *Phys. Rev. B* **64**, 224519 (2001).
  - [3] Yayu Wang *et al.*, *Phys. Rev. Lett.* **88**, 257003 (2002).
  - [4] Yayu Wang *et al.*, *Science*, **299**, 86 (2003).
  - [5] N. P. Ong and Yayu Wang, *Physica C* **408**, 11-14 (2004).
  - [6] J. Corson, R. Mallozzi, J. Orenstein, J. N. Eckstein, and I. Bozovic, *Nature* **398**, 221 (1999).
  - [7] S. Doniach and B. A. Huberman, *Phys. Rev. Lett.* **42**, 1169 (1979);
  - [8] C. Bergemann *et al.*, *Phys. Rev. B* **57**, 14387 (1998).
  - [9] M. J. Naughton, *Phys. Rev. B* **61**, 1605 (2000).
  - [10] J. Hofer *et al.*, *Phys. Rev. B* **62**, 631 (2000).
  - [11] D. C. Johnston and J. H. Cho, *Phys. Rev. B* **42**, 8710 (1990).
  - [12] M. Takigawa *et al.*, *Phys. Rev. B* **39**, 300 (1989); *ibid* *Phys. Rev. B* **43** 247 (1991).
  - [13] H. Alloul, A. Mahajan, H. Casalta, and O. Klein, *Phys. Rev. Lett.* **70**, 1171 (1993).
  - [14] In the UD sample, a fair question is whether the extrapolation should have a slight curvature. We estimate that this uncertainty adds at most an uncertainty of  $\pm 7\%$  in determining  $T_{onset}$ . However, because  $|M(T)|$  increases steeply below  $\sim 100$  K, the background uncertainty becomes increasingly insignificant for  $|M(T)|$ .
  - [15] Lu Li, Yayu Wang and N. P. Ong *et al.*, *Europhys. Lett.*, *in press*, cond-mat/050761.
  - [16] C. Carballera, J. Mosqueira, R. Revcolevschi, and F. Vidal, *Phys. Rev. Lett.* **84**, 3517 (2000).
  - [17] J. P. Gollub, M. R. Beasley, R. Callarotti, and M. Tinkham, *Phys. Rev. B* **7**, 3039 (1973).
  - [18] U. Welp *et al.*, *Phys. Rev. Lett.* **67**, 3180 (1991).
  - [19] Q. Li *et al.*, *Phys. Rev. B* **48**, 9877 (1993).
  - [20] V. G. Kogan *et al.*, *Phys. Rev. Lett.* **70**, 1870 (1993).
  - [21] C. Caroli, and K. Maki, *Phys. Rev.* **164**, 591 (1967).
  - [22] V. Oganessian, D. A. Huse and S. L. Sondhi, cond-mat/0502224.
  - [23] P. A. Lee, N. Nagaosa, X. G. Wen, cond-mat/0410445.
  - [24] V. J. Emery and S. A. Kivelson, *Nature* **374**, 434 (1995).
  - [25] P. W. Anderson, *Phys. Rev. Lett.* *in press*.
  - [26] P. A. Lee and X.-G. Wen, *Phys. Rev. B* **63**, 224517 (2001).
  - [27] For a review, see E. W. Carlson, V. J. Emery, S. A. Kivelson, D. Orgad, cond-mat/0206217.